Band offsets and heterostructures of two-dimensional semiconductors

Jun Kang,[1] Sefaattin Tongay,[2] Jian Zhou,[2] Jingbo Li,[1,a)] and Junqiao Wu[2,3,a)]
[1]*Institute of Semiconductors, Chinese Academy of Sciences, PO Box 912, Beijing 100083, People's Republic of China*
[2]*Department of Materials Science and Engineering, University of California, Berkeley, California 94720, USA*
[3]*Materials Sciences Division, Lawrence Berkeley National Laboratory, Berkeley, California 94720, USA*

(Received 7 November 2012; accepted 18 December 2012; published online 9 January 2013)

The band offsets and heterostructures of monolayer and few-layer transition-metal dichalcogenides MX_2 (M = Mo, W; X = S, Se, Te) are investigated from first principles calculations. The band alignments between different MX_2 monolayers are calculated using the vacuum level as reference, and a simple model is proposed to explain the observed chemical trends. Some of the monolayers and their heterostructures show band alignments suitable for potential applications in spontaneous water splitting, photovoltaics, and optoelectronics. The strong dependence of the band offset on the number of layers also implicates a possible way of patterning quantum structures with thickness engineering. © *2013 American Institute of Physics*. [http://dx.doi.org/10.1063/1.4774090]

After graphene became experimentally accessible in 2004,[1] two-dimensional (2D) materials have attracted great attention mainly due to their unique physical properties and capability to fulfill the demands of future nanoelectronic industry on flexibility, adaptability, and multi-functionality.[2] Transition metal dichalcogenides MX_2 (where M and X correspond to transition metal and chalcogen, respectively) are members of the layered materials like graphite. Soon after the discovery of graphene, it was demonstrated that monolayer MX_2, such as MoS_2 and $NbSe_2$, could also be achieved using mechanical exfoliation.[3] More recently, various experimental studies have reported the synthesis of MX_2 monolayers, such as MoS_2, WS_2, $MoSe_2$, $MoTe_2$, TiS_2, TaS_2, $TaSe_2$, $NiTe_2$, and ZrS_2.[4–6] Bulk MoX_2 and WX_2 are indirect band-gap semiconductors, whereas their monolayers have direct bandgaps,[7–9] which are favorable for optoelectronic applications. The existence of the native bandgap provides an excellent current on/off ratio of 10^8 in single-layer MoS_2 based field-effect transistors,[10] and the application of monolayer MoS_2 in integrated circuits and logic operations has already been realized.[11]

Recently, the band structure of single- and few-layer MX_2 has been studied using first principles *ab-initio* calculations, focusing mostly on their bandgap values, while their band offsets are much less explored. Band offsets of semiconductors are important and necessary parameters in material and device design. More specifically, the band offset is critical to many properties such as quantum confinement,[12] dopability,[13] and chemical activity.[14] Moreover, designing heterostructure devices based on 2D semiconductors requires accurate band offset parameters across different materials. Heterojunctions interfacing different 2D materials would enable the so-called van der Waals epitaxy,[15] in which the lattice matching condition in traditional epitaxy is drastically relaxed, allowing the formation of a wide range of 2D/2D, 2D/3D, or even more advanced 3D/2D/3D heterostructures. Finally, chemical trends of the band offsets provide a useful tool for predicting physical properties of materials and heterostructure geometries. Previously, the band offset between several bulk MX_2 has been investigated by Jiang.[16] However, due to the quantum confinement effect, the physical properties of the 2D semiconductors are very different compared to their 3D counterparts, and therefore the band offsets of single layer MX_2 are expected to show stark differences from the 3D case. So far, band offsets of monolayer MX_2 are completely unknown. In this work, we study the electronic properties of MX_2 monolayers and few layers (M = Mo, W, and X = S, Se, Te) using first principles calculations, but focus on their band offsets and interesting heterostructure geometries enabled by the band offsets. On the basis of the observed chemical trends, we discuss implications for potential device applications.

The calculations were performed using the Vienna *ab initio* simulation package (VASP).[17] The six outmost electrons for transition-metal and chalcogen were treated as valence electrons. The core-valence interaction was described by the frozen-core projector augmented wave (PAW) method.[18] The generalized gradient approximation of Perdew-Burke-Ernzerhof (GGA-PBE)[19] was adopted for exchange-correlation functional. Part of the calculations were also performed using the Heyd-Scuseria-Ernzerhof (HSE06) hybrid functional.[20] Energy cut off for plane-wave expansion was set to 400 eV. Brillouin zone sampling was performed with Monkhorst-Pack (MP) special k point meshes.[21] For the hexagonal unit cell, a grid of $24 \times 24 \times 1$ was used ($24 \times 24 \times 5$ in bulk calculations), and the k-point grid scaled with respect to the supercell size. A vacuum layer larger than 10 Å was added to avoid interaction between adjacent images. All atoms were allowed to relax until the calculated Hellmann-Feynman force on each atom was smaller than 0.01 eV/Å. Spin-orbit interaction (SOI) is included when calculating band structures. The vacuum level was taken as zero reference in the calculations of band alignment.

The monolayers of MX_2 considered in this work have hexagonal lattices with honeycomb structures (1 H-MX_2) similar to graphene. Basic lattice parameters and physical properties of single-layer MX_2 are listed in Table I, and the calculated bandgap values are consistent with previous studies.[9,22] Figure 1 shows the calculated band structure of

a)Authors to whom correspondence should be addressed. Electronic addresses: jbli@semi.ac.cn and wuj@berkeley.edu.

TABLE I. Calculated properties of MX_2 monolayers: lattice constant a, M-X bond length d, bandgap E_g, spin-orbit splitting Δ_{SO} in valence band, cohesive energy E_C per unit cell, charge transfer $\Delta\rho$ of the M atom, Poisson's ratio ν, and in-plane stiffness C. a, d, E_g, and Δ_{SO} calculated by HSE06 are also shown.

	a (Å)	a^{HSE} (Å)	d (Å)	d^{HSE} (Å)	E_g (eV)	E_g^{HSE} (eV)	Δ_{SO} (eV)	Δ_{SO}^{HSE} (eV)	E_C (eV)	$\Delta\rho$ (e)	ν	C (N/m)
MoS_2	3.18	3.16	2.41	2.40	1.59	2.02	0.15	0.20	15.31	1.09	0.25	124.24
$MoSe_2$	3.32	3.29	2.54	2.51	1.33	1.72	0.19	0.27	13.70	0.85	0.23	103.40
$MoTe_2$	3.55	3.52	2.73	2.70	0.94	1.28	0.22	0.35	12.01	0.52	0.24	78.90
WS_2	3.18	3.16	2.42	2.40	1.55	1.98	0.43	0.56	17.28	1.24	0.22	139.54
WSe_2	3.32	3.29	2.55	2.53	1.25	1.63	0.47	0.63	15.45	0.96	0.19	115.52
WTe_2	3.55	3.52	2.74	2.71	0.75	1.03	0.49	0.69	13.51	0.57	0.18	86.93

MoS_2, $MoSe_2$, and WS_2. While the lattice constants of monolayer MX_2 calculated by HSE06 are in excellent agreement with known bulk values, those obtained by PBE are slightly overestimated. Despite this slight discrepancy, we note that these two methods provide similar physical trends; i.e., when X goes from S to Te, the lattice constant and bond length of MX_2 increase associated with the increase in ionic radius of X. We also note that the lattice constants of MoX_2 and WX_2 are very close to each other, indicating that synthesizing MoX_2-WX_2 heterostructures might allow one to engineer optical and physical properties with minimum structural defects. Finally, elastic parameters which are obtained by fitting the strain-energy relationship of MX_2 monolayers show that the in-plane stiffness decreases when X changes from S to Te, and M changes from W to Mo. The calculated Poisson's ratios of MX_2 monolayer are around 0.2, and the Poisson's ratio of MoX_2 is found to be slightly larger than that of WX_2.

Previous studies have shown that MX_2 monolayers possess direct bandgaps, with the conduction band maximum (CBM) and valence band minimum (VBM) located at the K symmetry points,[7,9] as well as a significant spin-orbit splitting in valence band,[5,23] consistent with our results as listed in Table I. Comparing to the experimental values, we observe that the bandgap values are underestimated by PBE while they are slightly overestimated by HSE06. Here, we note that regardless of the choice of the method (PBE/HSE06), the observed general trends display similar behavior. Therefore, the deviation from the experimentally reported bandgap values can be omitted when comparing the band offsets between MX_2 monolayers, and hence the chemical trends of band structures of MX_2 can be properly described by both PBE and HSE06.

The band alignment for MX_2 monolayers is shown in Fig. 2(a). In the following, we discuss the results in Fig. 2 based on PBE calculations, but similar results can be deduced from the HSE06. Overall, the band offsets show the following trends:

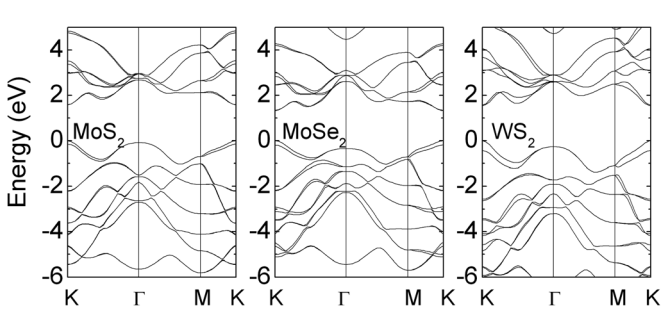

FIG. 1. Band structure of monolayer MoS_2, $MoSe_2$, and WS_2 calculated by PBE.

1. As the atomic number of X increases (from S to Te), the energies of CBM and VBM of MX_2 also increase. Moreover, the conduction band offset (CBO) is smaller than the valence band offset (VBO). More specifically, the VBM of $MoSe_2$ is 0.63 eV higher than that of MoS_2 while its CBM is 0.37 eV higher than that of MoS_2. Here, the only exception is WTe_2 where its CBM is slightly lower (by 0.06 eV) than that of WSe_2.
2. For common-X system, the CBM and VBM of WX_2 are higher than those of MoX_2, i.e., MoX_2-WX_2 lateral heterostructures have a type-II band alignment. For example, the VBM of WS_2 is 0.39 eV higher than that of MoS_2, and its CBM is 0.35 eV higher.

To understand the observed trends in the band offsets, we look at the physical origin of the observed CBM and VBM values. For simplifying, the following discussions are made based on the band structure calculated without SOI. (SOI only affects the CBM and VBM energies, while the general trends of the band offsets were found to be the same.) Taking MoS_2 as an example, the VBM of MoS_2 mainly consists of the $d_{x^2-y^2}$ and d_{xy} orbitals of Mo and the p_x and p_y orbitals of S. In addition, it is found that the 5th band at the K points, which locates about 4 eV lower than the VBM, has the same character as VBM. Therefore, the VBM of MoS_2 originates mainly from the repulsion between the $d_{x^2-y^2}$ and d_{xy} orbitals of Mo and the p_x and p_y orbitals of S. The d orbital of Mo is higher than the p orbital of S, so it is pushed up by Δ_1, forming the VBM, and the p orbital is pushed down by Δ_1', as shown in Fig. 2(b). The CBM of MoS_2 has the character of the d_{z^2} orbital of Mo and the p_x and p_y orbitals of S, while the 4th band at the K points, located about 4.5 eV lower than the VBM, has the same character. Thus, the CBM of MoS_2 originates from the repulsion between the d_{z^2} orbital of Mo and the p_x and p_y orbitals of S. The d_{z^2} orbital is pushed up by Δ_2, forming the CBM, and the p orbital is pusheddown by Δ_2'. Using this model, we can understand the trends of the band offsets of MX_2.

For common-M systems, the VBO and CBO are determined by the repulsion strength Δ_1 and Δ_2 between the cation d orbitals and anion p orbitals. The magnitude of the repulsion solely depends on the overlap integral of d and p orbitals and their difference in energy. In principle, a larger overlap integral or a smaller energy difference leads to larger

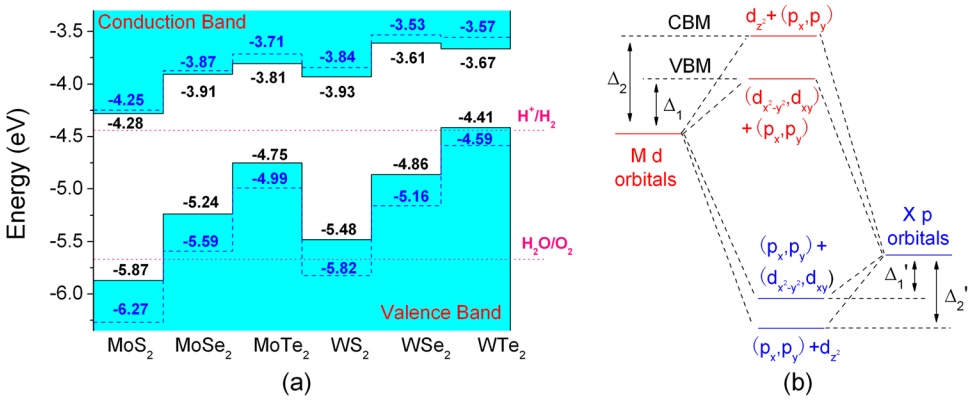

FIG. 2. (a) Calculated band alignment for MX_2 monolayers. Solid lines are obtained by PBE, and dashed lines are obtained by HSE06. The dotted lines indicate the water reduction (H^+/H_2) and oxidation (H_2O/O_2) potentials. The vacuum level is taken as zero reference. (b) Schematic of the origin of CBM and VBM in MX_2.

Δ value. For increasing X atomic number, its p orbitals become shallower. As a result, the anion with shallower p orbitals pushes the cation d orbitals upwards more than the anion with deeper p orbitals. As a result, Δ_1 and Δ_2 values are larger in systems with larger atomic number of X, and the CBM and VBM would be higher. However, when X goes from S to Te, the M-X bond length also increases. This would lead to a decrease of the overlap integral between the d and p orbitals, and partly counteract the increase of Δ_1 and Δ_2. It can be seen from Fig. 2(b) that the repulsion between M d_{z^2} and X p_x+p_y orbitals is stronger than that between M $d_{x^2-y^2}+d_{xy}$ and X p_x+p_y orbitals, possibly because the former has more σ bonding character while the latter has more π bonding character. Consequently, the influence of the decrease in overlap integral on Δ_2 is larger than that on Δ_1, and the increase of Δ_2 would be smaller than that of Δ_1. The presented interpretation provides an explanation for the general trend that the CBO is smaller than the VBO for common-cation systems. Particularly, W has high d orbitals, and the M-X bond length of WTe_2 is the largest among all MX_2. As a result, from WSe_2 to WTe_2, the influence of decrease in overlap integral on Δ_2 overrides the influence of increase in the anion p orbital energy, and Δ_2 decreases. So, the CBM of WTe_2 is lower than that of WSe_2.

The trends of band offset between common-X systems can be understood by the position of the d orbitals of cation. The energy of the 5 d orbital of W is higher than that of the 4 d orbital of Mo, therefore, the CBM and VBM of WX_2 are higher than those of MoX_2. Figure 2 shows that the band alignment between MoX_2 and WX_2 is type-II. In a type-II heterostructure, free electrons and holes will be spontaneously separated, which is suited for optoelectronics and solar energy conversion. Considering such possibility, we provide first calculations on MoX_2-WX_2 lateral heterostructures as shown in Fig. 3. We first note that MoX_2 and WX_2 have very similar lattice parameters (Table I), allowing one to create these heterostructures without inducing structural defects. Based on the distribution of charge densities, we observe that the electrons are confined in the MoX_2, while the holes are confined in the WX_2 side. It is, therefore, expected that spontaneous charge separation occurs when excitons diffuse to the WX_2/MoX_2 junction, a process that is needed for photovoltaics. In addition, superlattices formed by interfacing alternating WX_2 and MoX_2 layers would host mini-bands for quantum devices, and the band offset calculated here would be needed for the design.

It is well established that the bandgap of MX_2 is sensitive to its thickness,[7] thus its band offset would also be influenced by the thickness. The VBM and CBM positions of MX_2 for 1, 2, and 4 layers and bulk are shown in Fig. 4. We note that the calculated bulk band alignments are consistent with previous results based on PBE.[16] Generally speaking, as the number of layers is reduced, the VBMs of all MX_2 move downward (lower in energy), whereas the CBMs move upward (higher in energy), both of which can be understood from a simple quantum confinement effect. However, in some cases such as the VBM of WTe_2, this trend is not observed since the SOI, which would lift up the VBM, becomes weaker as the thickness increases. Figure 4 clearly shows that the band edge positions of 2D MX_2 are drastically different from the bulk cases, especially for MoS_2 and WS_2. Such differences could lead to possible applications of monolayer MX_2 in fields where their bulk counterparts are not suited. In addition, it is possible to pattern a MX_2 film into structures where different regions have different number of layers, thus achieving functional quantum devices by mere thickness engineering.

Another example is photo-splitting reactions of water. It is well known that to achieve high efficiency, the photocatalyst should satisfy two main conditions.[24] The first is the presence of an ideal bandgap (~2.0 eV) that allows absorption of a large portion of the solar spectrum. Among the

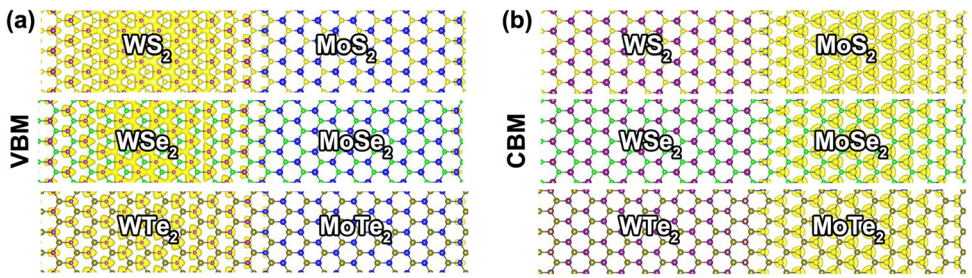

FIG. 3. Charge densities of VBM (a) and CBM (b) states for monolayer WX_2-MoX_2 lateral heterostructures with common X.

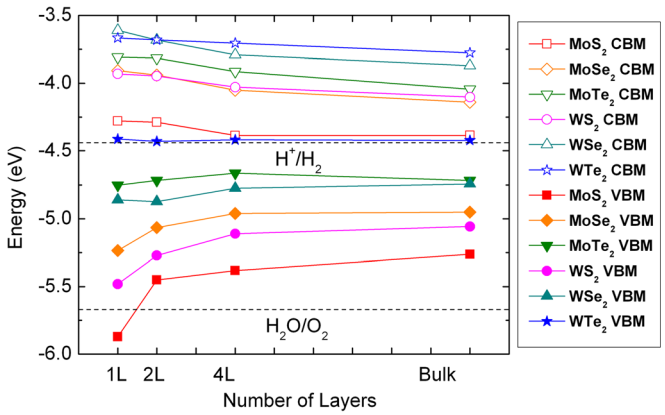

FIG. 4. Band edge positions of MX_2 as a function of the number of layers calculated by PBE. The vacuum level is taken as zero reference. The dashed lines indicate the water redox potentials.

MX_2 monolayers studied here, MoS_2 and WS_2 meet this condition. The second requirement is that the photocatalyst must have suitable band edges to straddle the redox potentials of water. The standard water redox potentials with respect to the vacuum level are -4.44 eV for the reduction (H^+/H_2), and -5.67 eV for the oxidation (H_2O/O_2).[25] Jiang has shown that bulk MX_2 cannot be applied directly to overall photo-splitting of water because their CBM or VBM positions are not suitable.[16] Our calculations show that indeed the CBMs (VBMs) of bulk MoX_2 and WX_2 are higher than the reduction (oxidation) potential (Fig. 4), so they can only be used for water reduction. However, according to Figs. 4(a), monolayer MoS_2 satisfies this band edge requirement. The energy of VBM of MoS_2 monolayer is calculated to be -5.87 eV by PBE and -6.27 eV by HSE06. Since PBE underestimates the bandgap while HSE06 overestimates, it is reasonable to expect that the actual VBM position of MoS_2 monolayer lies between -5.87 eV and -6.27 eV, which is lower than the water oxidation potential. The CBMs of MoS_2 calculated by PBE and HSE06 are both around -4.3 eV, higher than the water reduction potential. Therefore, MoS_2 monolayer is a good candidate for spontaneous photo-splitting of water. It should be noted that the idea of using nano MoS_2 for H_2 evolution is also proposed in several previous studies.[26] In these works, the activity of MoS_2 is mostly related to edge states or vacancies, hence the defect levels play important roles. Our calculations show that MoS_2 is suited for photo-splitting of water even in the absence of defects.

In summary, we have provided band offset calculations for various 2D semiconductors and investigated their elastic and electronic properties from first principles calculations. The calculated band offsets between MX_2 reveal that as the atomic number of M or X increases, the CBM and VBM energy also increases, and the VBO is larger than the CBO for common-cation pairs. We further show that the CBM and VBM of MX_2 originate from the repulsion between the cation *d* and anion *p* orbitals, and the chemical trends of the band offsets can be interpreted accordingly. The MoX_2-WX_2 lateral heterostructures have type-II band alignment, and are suited for optoelectronics and energy conversion, and MoS_2 monolayer is a good candidate for spontaneous photo-splitting of water.

J. Li gratefully acknowledges financial support from the Natural Science Foundation for Distinguished Young Scholar (Grant No. 60925016). This work was supported by the National Basic Research Program of China (Grant No. 2011CB921901) and the External Cooperation Program of Chinese Academy of Sciences. We acknowledge the computing resources provided by the Supercomputing Center, CNIC, CAS.

[1]K. S. Novoselov, A. K. Geim, S. V. Morozov, D. Jiang, Y. Zhang, S. V. Dubonos, I. V. Grigorieva, and A. A. Firsov, Science **306**, 666 (2004).
[2]C. Castro Neto and K. S. Novoselov, Mater. Express **1**, 10 (2011).
[3]K. S. Novoselov, D. Jiang, F. Schedin, T. J. Booth, V. V. Khotkevich, S. V. Morozov, and A. K. Geim, Proc. Natl. Acad. Sci. U.S.A **102**, 10451 (2005).
[4]J. N. Coleman, M. Lotya, A. O'Neill, S. D. Bergin, P. J. King, U. Khan, K. Young, A. Gaucher, S. De, R. J. Smith *et al.*, Science **331**, 568 (2011).
[5]S. Tongay, J. Zhou, C. Ataca, K. Lo, T. S. Matthews, J. Li, J. C. Grossman, and J. Wu, Nano Lett. **12**, 5576 (2012).
[6]Z. Zeng, Z. Yin, X. Huang, H. Li, Q. He, G. Lu, F. Boey, and H. Zhang, Angew. Chem., Int. Ed. **50**, 11093 (2011).
[7]K. Mak, C. Lee, J. Hone, J. Shan, and T. F. Heinz, Phys. Rev. Lett. **105**, 136805 (2010).
[8]W. S. Yun, S. W. Han, S. C. Hong, I. G. Kim, and J. D. Lee, Phys. Rev. B **85**, 033305 (2012).
[9]Y. Ding, Y. Wang, J. Ni, L. Shi, S. Shi, and W. Tang, Physica B **406**, 2254 (2011).
[10]B. Radisavljevic, A. Radenovic, J. Brivio, V. Giacometti, and A. Kis, Nat. Nanotechnol. **6**, 147 (2011).
[11]B. Radisavljevic, M. B. Whitwicj, and A. Kis, ACS Nano **5**, 9934 (2011).
[12]J. Li and L. Wang, Appl. Phys. Lett. **85**, 2929 (2004).
[13]S. B. Zhang, S. H. Wei, and A. Zunger, Phys. Rev. Lett. **84**, 1232 (2000).
[14]L. Kavan, M. Graetzel, S. E. Gilbert, C. Klemenz, and H. J. Scheel, J. Am. Chem. Soc. **118**, 6716 (1996).
[15]A. Koma, J. Cryst. Growth **201–202**, 236 (1999).
[16]H. Jiang, J. Phys. Chem. C **116**, 7664 (2012).
[17]G. Kresse and J. Furthmuller, Phys. Rev. B **54**, 11169 (1996).
[18]P. E. Blochl, Phys. Rev. B **50**, 17953 (1994).
[19]J. P. Perdew, K. Burke, and M. Ernzerhof, Phys. Rev. Lett. **77**, 3865 (1996).
[20]J. Heyd, G. E. Scuseria, and M. Ernzerhof, J. Chem. Phys. **118**, 8207 (2003).
[21]H. J. Monkhorst and J. D. Pack, Phys. Rev. B **13**, 5188 (1976).
[22]C. Ataca, H. Sahin, and S. Ciraci, J. Chem. Phys. C **116**, 8983 (2012).
[23]Z. Y. Zhu, Y. C. Cheng, and U. Schwingenschlogl, Phys. Rev. B **84**, 153402 (2011).
[24]Y. Gai, J. Li, S. S. Li, J. B. Xia, and S. H. Wei, Phys. Rev. Lett. **102**, 036402 (2009).
[25]V. Chakrapani, J. C. Angus, A. B. Anderson, S. D. Wolter, B. R. Stoner, and G. Sumanasekera, Science **318**, 1424 (2007).
[26]J. V. Lauritsen, J. Kibsgaard, S. Helveg, H. Topsøe, B. S. Clausen, E. Lægsgaard, and F. Besenbacher, Nat. Nanotechnol. **2**, 53 (2007); C. Ataca and S. Ciraci, Phys. Rev. B **85**, 195410 (2012); T. F. Jaramillo, K. P. Jørgensen, J. Bonde, J. H. Nielsen, S. Horch, and I. Chorkendorff, Science **317**, 100 (2007).